Selective Oxidation of 5-Hydroxymethylfurfural to 2,5-Diformylfuran by Visible Light-Driven Photocatalysis over In Situ Substrate-Sensitized Titania

Ayesha Khan,*[a] Michael Goepel,[b] Adam Kubas,[a] Dariusz Łomot,[a] Wojciech Lisowski,[a] Dmytro Lisovytskiy,[a] Ariadna Nowicka,[a] Juan Carlos Colmenares,*[a] and Roger Gläser*[b]

Solar energy-driven processes for biomass valorization are priority for the growing industrialized society. To address this challenge, efficient visible light-active photocatalyst for the selective oxidation of biomass-derived platform chemical is highly desirable. Herein, selective oxidation of 5-hydroxymethylfurfural (HMF) to 2,5-diformylfuran (DFF) was achieved by visible light-driven photocatalysis over titania. Pristine titania is photocatalytically inactive under visible light, so an unconventional approach was employed for the visible light ($\lambda = 515$ nm) sensitization of titania via a formation of a visible light-absorbing complex of HMF (substrate) on the titania surface. Surface-complexation of HMF on titania mediated ligand-to-metal charge transfer (LMCT) under visible light, which efficiently catalyzed the oxidation of HMF to DFF. A high DFF selectivity of 87% was achieved with 59% HMF conversion after 4 h of illumination. The apparent quantum yield obtained for DFF production was calculated to be 6.3%. It was proposed that the dissociative interaction of hydroxyl groups of HMF and the titania surface is responsible for the surface-complex formation. When the hydroxyl groups of titania were modified via surface-fluorination or calcination the oxidation of HMF was inhibited under visible light, signifying that hydroxyl groups are decisive for photocatalytic activity.

Introduction

Exploitation of renewable resources is crucial to ensure future energy demands and alleviate environmental problems. Biomass is a naturally abundant renewable resource, which has potential to partially replace fossil fuel-based feedstocks for sustainable production of fine chemicals.[1,2] To achieve this goal, the selective oxidation of biomass-derived platform chemicals into organic building blocks is a promising and desirable strategy.[3] 5-hydroxymethylfurfural (HMF) is a key bio-based platform chemical obtained from C_6 monosaccharides (derived from the depolymerization of cellulosic biomass),[4] which can be further converted into high value-added chemical such as 2,5-diformylfuran (DFF).[5,6] DFF has a broad range of potential applications as an intermediate for the synthesis of macrocyclic ligands, bio-based polymeric materials, pharmaceutical products, or antifungal agents etc.[7] Consequently, the selective oxidation of HMF to DFF has received considerable attention to date.[8–10]

Heterogeneous photocatalysis has great potential for the partial oxidation of HMF to DFF.[11] Specifically, visible light-driven photocatalytic conversion of HMF to DFF is an environmentally benign and economical approach compared to ultraviolet (UV) light-driven photocatalysis, which often is unselective (as it generates highly active oxidative species that over-oxidize the substrate)[12] and conventional thermocatalytic processes performed over costly noble metal catalysts at elevated temperatures (80–150 °C).[13] Until now, few studies were devoted to the partial oxidation of HMF to DFF under visible light using different semiconductor photocatalysts.[14] For example, Nb_2O_5 exhibited high selectivity for DFF (≈91%) at approximately 19% HMF conversion in benzotrifluoride after 6 h of illumination ($\lambda \geq 400$ nm).[15] In addition, photocatalytic oxidation of HMF performed using graphitic carbon nitride (g-C_3N_4) in aqueous medium achieved 40% HMF conversion and 50% DFF selectivity after 4 h of solar irradiation.[16] In another study, g-C_3N_4 in acetonitrile medium showed improved DFF selectivity (≈87%) with the HMF conversion of 31% after 6 h of irradiation ($\lambda > 400$ nm) under O_2 flow.[17] Although these semiconductors have demonstrated the practical applicability of visible light-driven photocatalysis for the transformation of HMF to DFF, the preparation of these photocatalysts (Nb_2O_5 and g-C_3N_4) involves high-temperature calcination (800 and ≈550 °C, respectively), which is not economical (due to high energy consumption).

[a] A. Khan, Prof. A. Kubas, Dr. D. Łomot, Dr. W. Lisowski, Dr. D. Lisovytskiy, Dr. A. Nowicka, Prof. J. C. Colmenares
Institute of Physical Chemistry
Polish Academy of Sciences
Warsaw 01-224 (Poland)
E-mail: akhan@ichf.edu.pl
jcarloscolmenares@ichf.edu.pl
[b] Dr. M. Goepel, Prof. Dr. R. Gläser
Institute of Chemical Technology
Leipzig University
Leipzig 04103 (Germany)
E-mail: roger.glaeser@uni-leipzig.de

Supporting information for this article is available on the WWW under https://doi.org/10.1002/cssc.202002687

Henceforth, the quest for a cost-effective, chemically stable, and efficient visible light-responsive photocatalyst is actively pursued for the selective oxidation of HMF to DFF. Titania is a widely used, inexpensive, and efficient photocatalyst employed in various environmental and industrial applications.[18,19] However, its application in organic transformations is limited by the wide bandgap (≈3.2 eV), which requires UV light (accounts for <5% of solar radiation) for photoactivation.[19,20] Notably, pristine titania is considered to be highly unselective for the oxidation of HMF, which was attributed to the over-oxidation of the target products.[15] The highest selectivity to DFF achieved by pristine titania until now is only 22% at 50% HMF conversion in an aqueous medium under UV light ($\lambda = 365$ nm) irradiation.[21] Therefore, modifying the optical response of titania to the visible light (accounts for ≈45% of solar radiation[19]) range will make the application of photocatalysis more economical and environment friendly for the production of industrially relevant chemicals like DFF.

Numerous strategies have been used to tune the absorption of titania toward the visible light region including metal (Fe,[22] V,[23] Ni[24]) or non-metal (N,[25] S,[26] C[27]) doping and coupling titania with dyes (dye sensitization)[28] or narrow bandgap semiconductors such as CdS and WO_3.[29] Another strategy that has been much less investigated is the ligand-to-metal charge transfer (LMCT) by complex formation on the titania surface. In this approach, the adsorbates or substrates (which do not absorb visible light themselves) form a surface-complex on titania. The resulting complex serves as a visible light sensitizer and induces charge transfer from the highest occupied molecular orbital (HOMO) of the adsorbates to the conduction band (CB) of titania upon visible light irradiation.[19]

Various organic compounds with hydroxyl functional group (glucose, benzyl alcohol, phenol, catechol, chlorophenols, ascorbic acid, etc.) and carboxylic acid functional group (formic acid, citric acid, lactic acid, etc.) can form LMCT complexes on titania, accompanied by the absorption of visible light,[19] which is not exhibited by either adsorbates and titania alone. Several studies have been carried out to investigate the LMCT-mediated photocatalytic activity of surface-complexed titania under visible light. Catechol surface-complexed titania is a typical example, which extends the optical absorption of titania into the visible light region (up to 600 nm). As a photocatalyst, catechol-on-titania efficiently and selectively oxidizes amines (with 55% conversion) into imines (with 90% selectivity) ascribed to visible light-induced interfacial charge transfer.[30] In addition, 2,4,5-trichlorophenol can also form a charge-transfer complex on titania (P25) that is activated by light wavelengths as long as 520 nm. The resulting charge-transfer complex forms trichlorophenoxyl radicals, which upon coupling form polyaromatic chlorinated products under visible light.[31,32] Higashimoto et al.[33] reported that benzyl alcohol on titania is oxidized into its corresponding aldehyde (benzaldehyde) with 99% selectivity under visible light via LMCT complex formation.[33,34] Formation of LMCT complex between the titania surface and substrate presents a significant potential for the development of solar-driven photocatalytic systems.

Herein, we investigate the LMCT-mediated photocatalytic activity of titania, prepared through sol-gel and hydrothermal-assisted method (SGH-TiO_2) for the selective oxidation of HMF to DFF under visible light ($\lambda = 515$ nm). It has been found that the adsorption of substrate (HMF) on SGH-TiO_2 surface enabled the formation of a visible light-absorbing complex. The resulting complex mediates LMCT under visible light and the electrons transferred from the surface-complex to the CB of the SGH-TiO_2 activate molecular oxygen and catalyze the oxidation of HMF to DFF. This work provides a better understanding of visible light sensitization of titania via LMCT approach and also demonstrates its promising potential for the selective oxidation of biomass-derived platform chemicals.

Results and Discussion

Characterization

The comparison of XRD patterns of SGH-TiO_2 and P25 is shown in Figure S1a,b in the Supporting Information. The XRD reflexes observed at 25.4 (101), 37.9 (004), 48.0 (200), 54.4 (105), 63.2 (204), 69.3 (116), and 75.7° (215) correspond to the anatase phase of titania (JCPDS Card No. 21–1272)[35] in both SGH-TiO_2 and P25 (Figure S1a,b, Supporting Information), whereas the XRD reflex appearing at 30.8° (121) in SGH-TiO_2 was assigned to the brookite phase of titania (JCPDS no. 29-1360).[36] On the other hand, P25 showed (Figure S1b, Supporting Information) distinct reflexes at 27.3 (110), 36.1 (101), 41.2 (111), 53.9 (211), and 56.6° (220), which are characteristic of the rutile phase of titania (JCPDS card no. 21-1276).[35] The obtained results for phase composition and crystallite size are presented in Table 1. Textural properties of SGH-TiO_2 and P25 evaluated by N_2 sorption isotherms (Figure S2a,b, Supporting Information) showed that SGH-TiO_2 exhibited a type IV isotherm with H2 hysteresis, which is characteristic of mesoporous materials. P25 exhibited a type II isotherm with H3 hysteresis indicative of plate-like particles or assemblages of slit-shaped pores.[37] The microstructure properties such as specific surface area, pore volume, and pore width (Figure S2c,d, Supporting Information) of SGH-TiO_2 and P25 are summarized in Table 1. Morphology, phase composition, and average particle size of the as-

Table 1. Textural [Brunauer-Emmett-Teller specific surface area (SSA); Barrett-Joyner-Halenda pore volume (BJH V_p) and pore width (BJH w_p)] and crystallographic (phase composition and crystal size) properties of SGH-TiO_2.

Sample	Ratio of crystalline phases (anatase:brookite:rutile) [%]	Crystal size [nm] Anatase	Brookite	Rutile	SSA [$m^2 g^{-1}$]	BJH V_p [$cm^3 g^{-1}$]	BJH w_p [nm]
SGH-TiO_2	74:26:0	5	6		177	0.20	3
P25	87:0:13	17		24	53	0.22	16

synthesized SGH-TiO_2 nanoparticles were further corroborated by TEM analysis. TEM characterization of SGH-TiO_2 showed that the as-prepared SGH-TiO_2 nanoparticles consist of anatase and brookite phase (Figure S3a, Supporting Information), with small crystal size less than 10 nm (Figure S3b, Supporting Information). Furthermore, the lattice spacing (Figure S3c, Supporting Information) of 0.347, 0.290, and 0.351 nm corresponds to the (111), (121), and (120) crystal planes of brookite, respectively,[38] whereas the lattice spacing of 0.352 nm is ascribed to the (101) crystal plane of anatase.[39] The hydroxyl group density (OH nm^{-2}) based on thermogravimetric analysis (TGA) weight loss (Figure S4, Supporting Information) of SGH-TiO_2 and P25 is calculated to be 9 and 7 OH nm^{-2}, respectively. The results obtained are comparable with the literature-reported OH group density of P25 (8 OH nm^{-2},[40] 5.3 OH nm^{-2}[41]) and sol-gel-prepared titania (10.2 OH nm^{-2},[42] 8.7 OH nm^{-2},[43] and 11.9 OH nm^{-2}[44]).

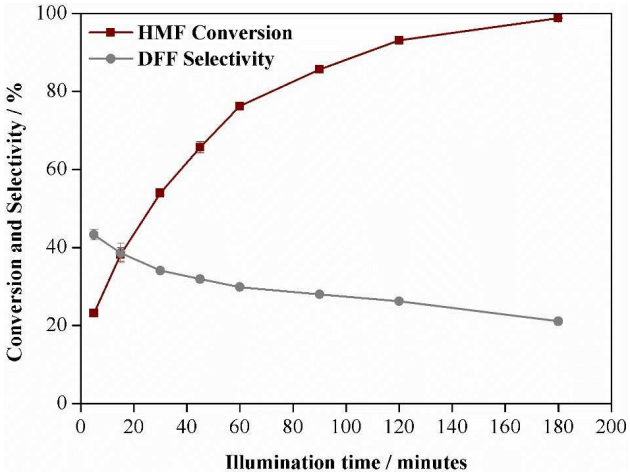

Figure 1. Conversion of HMF and selectivity for DFF in the photocatalytic oxidation of HMF to DFF in an acetonitrile medium over SGH-TiO_2 under UV light ($\lambda = 375$ nm).

Photocatalytic behavior of SGH-TiO_2

The photocatalytic performance of SGH-TiO_2 was investigated for the selective oxidation of HMF to DFF in acetonitrile under UV light ($\lambda = 375$ nm). SGH-TiO_2 exhibited a high photocatalytic activity with 52% HMF conversion and 36% DFF selectivity after 30 min of illumination under UV light (Figure 1). Besides DFF, no other intermediate compounds were detected. However, very low DFF selectivity (36%) indicated that the photocatalytic oxidation of HMF may proceed at two different active sites, through two parallel pathways:[21] i) partial oxidation of HMF to DFF that is desorbed from the catalyst surface and may compete with HMF for further oxidation and lead to mineralization; (ii) complete oxidation of HMF to CO_2 and H_2O through intermediates that do not release from the catalyst surface to liquid phase. This is in agreement with the study carried out by Yurdakal et al.[21] who compared different crystalline phases of titania for the selective oxidation of HMF to DFF under UV light in aqueous medium.

To explore the influence of incident light wavelengths, the photocatalytic reaction was also performed under visible light ($\lambda = 515$ nm). Interestingly, SGH-TiO_2 exhibited a high photocatalytic activity also under visible light, with 59% HMF conversion and 87% DFF selectivity after 4 h of illumination (entry 2, Table 2). The selectivity of the DFF increases gradually in the beginning (Figure 2a), which may have ascribed to the slow desorption of DFF from the catalyst surface. Moreover, DFF

Table 2. Results of the photocatalytic oxidation of HMF under different conditions.[a]

Entry	Photocatalyst	Light	Additive	HMF Conv. [%]	DFF Sel. [%]	DFF Yield [%]	Carbon balance [%]
1	SGH-TiO_2	UV[b]	none	52	36	19	66
2	SGH-TiO_2	visible	none	59	87	52	92
3	P25	visible	none	18	69	12	94
4	none	visible	none	0	0	0	100
5	SGH-TiO_2-cal-600	visible	none	0	0	0	100
6	F-SGH-TiO_2	visible	none	0	0	0	100
7	P90	visible	none	35	75	26	91
8	SGH-TiO_2	visible	methanol	56	88	48	93
9	SGH-TiO_2	visible	BQ	0	0	0	100
10	SGH-TiO_2	visible	Ag^+	0	0	0	100
11	SGH-TiO_2	visible	Ar[c]	0	0	0	100
12	SGH-TiO_2	visible	air	52	96	50	98
13	SGH-TiO_2	visible	Ar:air	38	87	33	97
14	SGH-TiO_2	dark	none	0	0	0	100
15	SGH-TiO_2[d]	visible	none	0	0	0	100
16	SGH-TiO_2[e]	visible	none	0	0	0	100
17	anatase	visible	none	0	0	0	100
18	brookite	visible	none	0	0	0	100
19	Ana:brook (74:26)	visible	none	0	0	0	100

[a] Reaction conditions: HMF (1 mM, 0.02 mmol), photocatalyst (1 g L^{-1}, 20 mg), scavenger (1:1 molar ratio of substrate, 0.02 mmol), reaction time (4 h). [b] Reaction time: 30 min; reaction medium: acetonitrile. [c] Reaction medium: degassed acetonitrile. [d] Reaction medium: water. [e] Reaction medium: 90:10 acetonitrile/water. HMF solution volume: 20 mL; air flow rate: 25 mL min^{-1}, 21% O_2; Ar flow rate: 25 mL min^{-1}, 99.9% Ar; Ar:air flow rate: 15 mL min^{-1}:10 mL min^{-1}, 60% Ar and 8.4% O_2); incident light wavelength: UV: 375 nm, visible: 515 nm; incident light intensity: ≈54 W m^{-2} (6× ≈9 W m^{-2}); ana:brook: physical mixture of anatase and brookite.

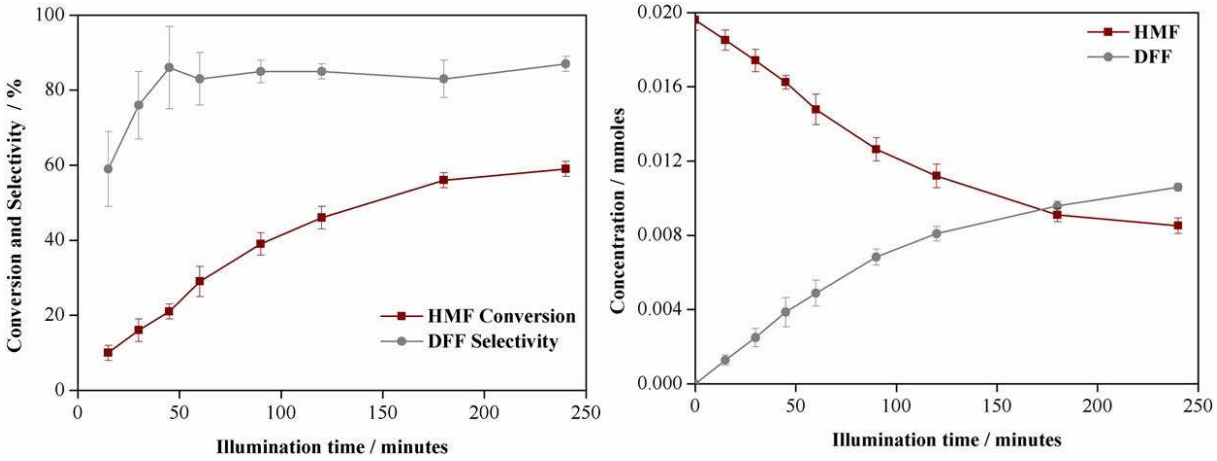

Figure 2. (Left) Conversion of HMF and selectivity for DFF in the photocatalytic oxidation of HMF to DFF over SGH-TiO_2 under visible light ($\lambda = 515$ nm). (Right) Oxidation of HMF and production of DFF over SGH-TiO_2 as a function of time over SGH-TiO_2.

selectivity remains stable under visible light during the course of reaction (Figure 2a), which suggests that the low-energy visible light radiation inhibits the over-oxidation of DFF.

The oxidation of HMF over SGH-TiO_2 as a function of time (Figure 2b) showed that the HMF was oxidized rapidly in the beginning; the initial reaction rate observed after 60 min of illumination was 8.02×10^{-5} mmol min^{-1}. The oxidation of HMF slowed down with time, which may correspond to the deactivation of the active sites of the catalyst.[10] However, no titanium leaching was observed after 4 h of photocatalytic reaction. Commercial TiO_2 (P25) was also tested in our reaction system, which showed very low HMF conversion (18%) with 69% DFF selectivity (entry 3, Table 2) after 4 h of illumination. It is noteworthy that both photocatalysts (SGH-TiO_2 and P25), in principle active only under UV light, showed activity under visible light ($\lambda = 515$ nm). This suggests that they either follow a special mechanism under visible light or possess unique features that impart visible light sensitivity.

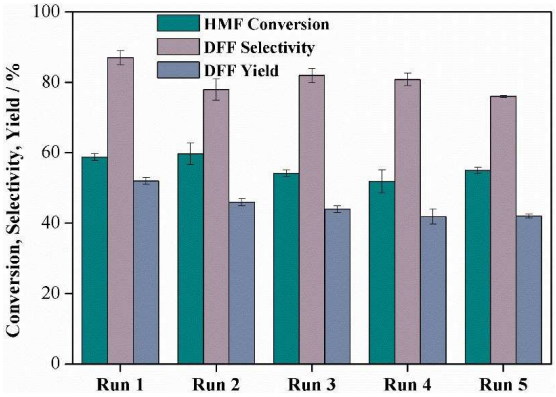

Figure 3. Cycling runs for the photocatalytic oxidation of HMF over SGH-TiO_2 under visible light irradiation.

Recycling test of SGH-TiO_2 for HMF oxidation

The stability and recyclability of the photocatalyst is of great importance from the industrial application point of view. To investigate the reusability of the catalyst, the recycling experiment was carried out for the photocatalytic oxidation of HMF using SGH-TiO_2. As shown in Figure 3, SGH-TiO_2 can be used in multiple cycles without substantial drop in the HMF conversion and DFF selectivity.

Apparent quantum yield measurement

The photon flux absorbed by the photocatalytic system is calculated to be 11.63×10^{-9} einsteins s^{-1}. The apparent quantum yields (AQY) exhibited by SGH-TiO_2 and P25 for DFF production after 4 h of illumination were calculated to be 6.3 and 2.2% at a wavelength of 515 nm, respectively, which are comparable to the reported efficiency of titania (4.3%) for the selective oxidation of benzyl alcohol under visible light (500 nm).[33]

Formation of LMCT complex on SGH-TiO_2

A series of characterizations was carried out to explore the underlying reason accounting for the photocatalytic activity of SGH-TiO_2 and P25 for the oxidation of HMF under visible light. We first examined the effect of HMF adsorption on the absorption spectrum of the SGH-TiO_2 and P25. For this purpose, diffuse reflectance (DR-)UV/Vis absorption spectra of SGH-TiO_2, P25, HMF-adsorbed SGH-TiO_2 (HMF-Ads-SGH-TiO_2), and HMF-adsorbed P25 (HMF-Ads-P25) in acetonitrile (under the same photocatalytic reaction conditions) were recorded. The DR-UV/Vis absorption spectra (Figure 4) show that the adsorption of HMF on P25 extended the absorption in the visible light region with the slight change in color of P25 (Figure 4). The adsorption of HMF on SGH-TiO_2 induces a marked increase in the visible

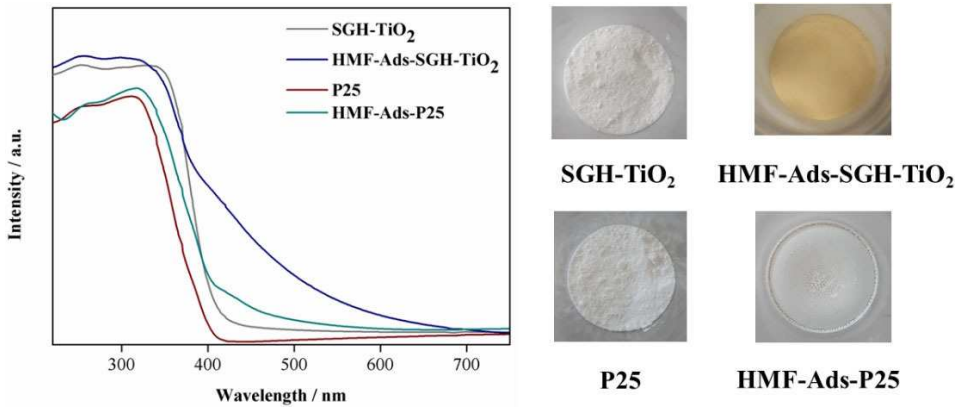

Figure 4. DR-UV/Visible absorption spectra of SGH-TiO_2, P25, HMF-Ads-SGH-TiO_2, and HMF-Ads-P25.

light absorption up to 650 nm, which is also accompanied by a significant change in color of SGH-TiO_2 (from white to yellow, Figure 4). Interestingly, HMF itself does not absorb light in the visible region like titania. It is therefore hypothesized that the visible light absorption results from the surface interaction of HMF and SGH-TiO_2. To test this hypothesis, a control experiment performed in the absence of SGH-TiO_2 showed no activity, confirming that the reaction was not occurring through direct photoactivation of the HMF (entry 4, Table 2).

To further investigate that the phenomenon of extended absorption in the visible region has occurred due to the interaction of HMF with the titania surface, Fourier-transform (FT)IR analysis was performed for HMF, SGH-TiO_2, and HMF-Ads-SGH-TiO_2 samples. The distinguishing differences in the spectrum of HMF-Ads-SGH-TiO_2 compared to individual components can be seen in Figure S5 in the Supporting Information. The bands appearing in HMF-Ads-SGH-TiO_2 sample at 1662, 1537, and 1420 cm^{-1} are characteristic IR bands for HMF, assigned to C=O stretching vibration, symmetric stretching of the C=C bonds, and asymmetric stretching of the C=C bonds, respectively.[45] This suggests that HMF may have adsorbed on the surface of SGH-TiO_2. A weak band at 1198 cm^{-1} in the HMF-Ads-SGH-TiO_2 spectrum corresponds to C–C–C multiple rocking vibrations.[15] Interestingly, the band corresponding to the O–H stretching vibrations in HMF and SGH-TiO_2 [hydroxyl species present in the form of free or H-bonded water or metal (Ti) hydroxyl groups] at 3200–3400 cm^{-1} is absent in the HMF-Ads-SGH-TiO_2 spectrum. The lack of an observable O–H stretching band in the HMF-Ads-SGH-TiO_2 spectrum is an indication that the adsorption of HMF on SGH-TiO_2 occurred through the –OH group on the metal surface forming a metal alkoxide complex. Moreover, the characteristic band of titania owing to the Ti–O–Ti and Ti–O–C stretching vibration in the range of 800–400 cm^{-1} has also been observed for HMF-Ads-SGH-TiO_2. The bands appearing at 2357 and 2115 cm^{-1} in SGH-TiO_2 and HMF-Ads-SGH-TiO_2 spectra are ascribed to physically adsorbed CO and CO_2, respectively.

Raman spectra (Figure S6, Supporting Information) have also been recorded for HMF, SGH-TiO_2, and HMF-Ads-SGH-TiO_2 to further corroborate the surface interaction of HMF and SGH-TiO_2. As seen in Figure S6b in the Supporting Information, the HMF-Ads-SGH-TiO_2 spectrum contained characteristic C=C symmetric vibrations of the furan ring at 1521 cm^{-1},[46] which indicates the adsorption of HMF on SGH-TiO_2 surface. Besides that, the broad band corresponding to the O–H stretching vibrations at 3200–3400 cm^{-1} (Figure S6c, Supporting Information) in SGH-TiO_2 and HMF spectra completely disappeared in HMF-Ads-SGH-TiO_2, suggesting the formation of a LMCT complex via a dissociative adsorption of the CH_2OH group of HMF and OH group of SGH-TiO_2. Additionally, the HMF-Ads-SGH-TiO_2 spectrum showed a weak band at 2941 cm^{-1}, which is assigned to C–H stretching vibrations.[47] A broad doublet appearing at 1637 and 1680 cm^{-1} may correspond to C=O stretching vibrations associated to HMF. Moreover, the HMF-Ads-SGH-TiO_2 spectrum showed a new weak band at 1048 cm^{-1}, which may have attributed to the C–O stretching of the alcoholate species formed between SGH-TiO_2 and HMF. These results indicated that the HMF molecules interact with the SGH-TiO_2 and formed a surface complex. Apart from that, Raman spectra of HMF-Ads-SGH-TiO_2 also confirmed the presence of three characteristic Raman active modes of the anatase phase of titania (Figure S6a, Supporting Information) at 399, 513, and 635 cm^{-1} that are assigned to B_{1g}, A_{1g}/B_{1g} (unresolved doublet), and E_g symmetries, respectively.[48] A strong band at 152 cm^{-1} corresponds to the A_{1g} mode of brookite.[49]

X-ray photoelectron spectroscopy (XPS) measurements were recorded to obtain information about the changes in the chemical environment of the surface of SGH-TiO_2 after the interaction of HMF. The XPS spectrum of SGH-TiO_2 shows (Figure S7a, Supporting Information) that the Ti 2p split well into four peaks: Ti $2p_{3/2}$ at 458.5 eV and Ti $2p_{1/2}$ at 464.3 eV are consistent with Ti^{4+} in TiO_2 lattice.[15] Ti $2p_{3/2}$ at 457.0 eV and Ti $2p_{1/2}$ at 462.8 eV correspond to Ti^{3+} in Ti_2O_3.[50] This indicates the presence of both $Ti^{4+}$and Ti^{3+} in SGH-TiO_2. When compared with HMF-Ads-SGH-TiO_2, the high-resolution XPS spectrum of Ti 2p did not show a prominent shift in the binding energies and variation in the peak area (Figure S7b, Supporting Information). This suggests that the electronic state of Ti element has not changed after HMF adsorption. Moreover, after

the adsorption of the HMF the peak area of Ti^{4+} decreased negligibly (≈1%) and that of Ti^{3+} increased by approximately 1%, which accounts for a stable titania lattice and indicates the probable interaction of HMF via a terminal OH groups rather than the substitution of Ti. The O 1 s spectrum of SGH-TiO_2 (Figure S7c, Supporting Information) is deconvoluted into four peaks. The peak at 529.7 eV is attributed to lattice oxygen, whereas the peaks at 530.5 and 531.3 eV correspond to oxygen bound to titanium in Ti_2O_3 and oxygen bound to carbon (C=O), respectively. The peak at 532.8 eV corresponds to hydroxyl groups bound to titanium or carbon (Ti–OH or C–OH). When compared with the O 1 s spectrum of HMF-Ads-SGH-TiO_2 (Figure S7d, Supporting Information), the peak previously corresponding to surface-bound oxygen in the form of hydroxyl groups slightly shifted to lower binding energy (532.5 eV). This may have ascribed to slightly higher electron density[15] around OH group-associated oxygen after the adsorption of HMF. However, there is a negligible increase in the peak area of O 1 s associated to lattice and surface-bound oxygen after HMF adsorption (Figure S7d, Supporting Information).

To gain further insight into the HMF adsorption process at the titania surface, we performed state-of-the-art quantum chemical calculations. Here, we used a neutral, hydrogen-terminated $[Ti_{20}O_{62}H_{44}]^0$ cluster to represent the anatase (101) surface (Figure S8, Supporting Information). It was recently shown that clusters of this size provide adsorption energies close to the periodic values.[51] However, finite cluster approach allows to use high-level methods such as DLPNO-CCSD(T)[52,53] extrapolated to complete basis set limit (CBS) to get highly accurate results as shown for the adsorption of small molecules on anatase[51] and rutile[54] surfaces. H-termination instead of point charge embedding made the geometry optimization step and zero-point energy (ZPE) correction straightforward at the more economic DFT/PBE level. Thus, the energies reported are single-point DLPNO-CCSD(T)/CBS energies at the DFT/PBE geometries and include ZPE corrections. Our calculations show the interaction of HMF with the model surface is overall downhill in energy (Figure 5a). Chemisorption is exothermic (−2.70 eV) due to H-bond formation between –OH group of the HMF and O center at the TiO_2 terrace accompanied with C=O→Ti coordination. Additionally, the titania surface interacts with the π system of the HMF molecule via dispersion forces (C state, Figure 5a; detailed structure is shown in Figure S9, Supporting Information). Subsequently, 0.57 eV is released upon O–H heterolytic bond cleavage (D state, Figure 5b). This results in a strong covalent bond formation between HMF's oxygen and the titanium atom (bond length of 1.82 Å). According to the computed IR spectrum (Figure 5e), the presence of C–O···Ti stretching vibrations should be visible just above 1000 cm^{-1}, while the peak above 1500 cm^{-1} is ascribed to C=C ring vibrations and should be broadened by unequal interactions at opposite sides of the ring. The former is experimentally obscured by TiO_2 lattice vibrations, but the latter is clearly visible in the experimental spectrum (Figure S5, Supporting Information). Regarding the Raman spectra (Figure 5f), our calculations show that symmetric C=C stretch of the furan ring will have significantly higher intensity as compared to the same mode of vibration detectable in IR spectra. This trend is evident also in the experimental spectrum (Figure S6, Supporting Information). Moreover, distinct features between 1350–1400 cm^{-1} are associated with the symmetric ring vibrations accompanied with vibration of the CH_2 group in the $–CH_2–O–Ti$ group (rocking and wagging).

Analysis of the PBE0 frontier molecular orbitals (Figure 5c,d) of state D reveals that the HOMO is located at the HMF moiety while the lowest unoccupied orbital (LUMO) is delocalized between HMF and a combination of Ti d orbitals (TiO_2 d-band). Thus, the basic HOMO→LUMO transition will have LMCT character although the computed HOMO-LUMO gap here is still significant and varies between 2.4 and 4.2 eV at PBE and PBE0 level, respectively. Such variation is not exceptional as the bandgap width is known to be functional-dependent.[55] More-

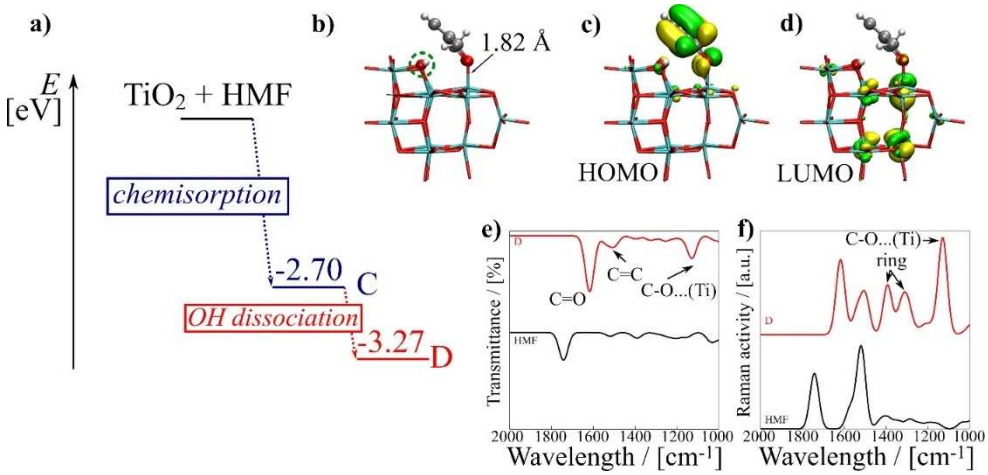

Figure 5. Theoretical analysis of HMF adsorption on TiO_2 anatase (101) model surface. (a) Energetics of the process with a breakdown into two consecutive steps: chemisorption (blue, C, dative C=O→Ti bond formation) and OH dissociation (red, D, O–Ti covalent bond formation). The structure of the state D is shown in panel (b) while the corresponding HOMO and LUMO are shown in panels (c) and (d), respectively (±0.03 a.u. isosurface). Simulated IR (e) and Raman (f) spectra change upon D state formation in comparison to free HMF in the 1000–2000 cm^{-1} region.

over, the HOMO-LUMO gap of the cluster should only be considered as zero-order approximation to the true solid-state bandgap. Interestingly, we found about 0.5 eV singlet-triplet gap decrease upon HMF dissociative adsorption: T_1-S_0 energy difference at the PBE0 level is 3.03 and 2.53 eV for free HMF and state D, respectively. We note that in the triplet D state the unpaired electron density resides mainly at the HMF moiety (1.92 *e* according to Löwdin population analysis) with only minor delocalization onto TiO_2 cluster. 2.5 eV corresponds to approximately 500 nm excitation wavelength but the accessibility of T_1 state will strongly depend on the spin-orbit coupling matrix element $H_{SOC} = <S_0|H_{SOC}|T_1>$. We used complete active space self-consistent field (CASSCF) approach to estimate H_{SOC} and found it to be 0.07 and 0.94 cm^{-1} for free HMF and state D, respectively. Therefore, as the probability of $T_1 \leftarrow S_0$ transition is in proportion to the $|H_{SOC}|^2$ we expect at least an order of magnitude increase of this transition probability upon HMF adsorption at the titania surface. This may indicate a possible role of triplet states in LMCT process.[56] However, further investigation of this phenomenon is beyond the scope of the current study.

Role of surface OH groups for photocatalytic activity of SGH-TiO_2

In order to further elucidate the contribution of the surface hydroxyl group in LMCT complex formation, SGH-TiO_2 was calcined at 600 °C for 3 h in air with the aim to remove surface hydroxyl groups by condensation. FTIR (Figure S10, Supporting Information) and Raman (Figure S11, Supporting Information) spectra of the as-calcined SGH-TiO_2 sample (SGH-TiO_2-cal-600) exhibited that the band corresponding to O–H stretching (3200–3400 cm^{-1}) and bending vibrations (1333 cm^{-1}) disappeared upon calcination. However, the calcined titania (SGH-TiO_2-cal-600) was inactive as a catalyst for the oxidation of HMF under visible light (entry 5, Table 2), signifying that hydroxyl groups are decisive for photocatalytic activity. They are likely involved in the visible light-active LMCT complex formation.

In a further approach to study the role of the OH-groups for photocatalytic activity, SGH-TiO_2 was chemically modified via a surface-fluorination to replace the surface hydroxyl groups with F^- ions.[57] The surface coverage of F^- ion is calculated to be 7 OH nm^{-2}, which corresponds to approximately 80% of the F^- ion surface exchange with the hydroxyl groups. The XPS analysis of surface-fluorinated SGH-TiO_2 (F-SGH-TiO_2) also confirmed that the F^- ions are adsorbed on the TiO_2 surface and the surface OH groups of TiO_2 were modified to Ti–F (Table S1, Supporting Information). In addition, the lack of an observable O–H stretching band in the FTIR (Figure S10, Supporting Information) and Raman (Figure S11, Supporting Information) spectra of F-SGH-TiO_2 further corroborate the exchange of terminal OH groups with F^- ions. As expected, surface-fluorination completely blocked the activity of SGH-TiO_2 (entry 6, Table 2). This is again consistent with inhibiting the adsorption of the substrate (HMF) on the titania surface and, thus, the formation of the LMCT complex through hydroxyl group interaction.

Active sites and conversion per surface OH group

In the field of catalysis, the term "active site" is often employed for the adsorption site effective for catalytic reactions. For a photocatalytic reaction it is often used for the dispersed chemical species such as metal complexes or adsorbed chemical species on the support.[58] However, the photocatalytic reaction can take place only upon the absorption of light by these species, and non-irradiated species cannot act as an active site.[58–60] Therefore, the term "active site" is sometimes misleading in photocatalysis, and its correlation with photocatalytic activity is hard to predict.[58] Nevertheless, the estimation of photocatalytic activity on the basis of number of active sites cannot be completely ruled out. Here, the hydroxyl groups of the titania surface are considered to be the potential active sites. Therefore, the photocatalytic activity was also evaluated using the number of molecules of HMF converted after 1 h of illumination and the number of initially present OH groups. Table 3 shows the conversion of HMF with respect to surface OH groups and area-related parameters. The number of OH groups on SGH-TiO_2 surface was found to be four times higher than P25 (Table 3). However, the area-normalized rate (conversion of HMF per surface OH groups per unit time) observed for P25 was 1.5 times higher than SGH-TiO_2. P25 showed two times higher conversion of HMF per surface OH groups than SGH TiO_2. Nevertheless, there are a number of factors that may affect the conversion of HMF per surface OH groups. The lower conversion of HMF per surface OH groups by SGH TiO_2 may indicate that all the OH groups are not necessarily accessible to HMF for adsorption to activate the catalytic cycle. Additionally, the whole surface area is not accessed by light, especially inside the pores and aggregated particles.[61]

Table 3. Area-normalized conversion, area-normalized rate, conversion per surface OH groups, and conversion per surface OH groups per unit time achieved by SGH-TiO_2 and P25.[a]

Catalyst	Area-normalized Conv. [m^{-2}]	Area-normalized rate [$m^{-2}s^{-1}$]	D_{OH} [nm]	Number of OH groups	Conv. OH^{-1}	Conv. $OH^{-1}s^{-1}$
SGH-TiO_2	8.1×10^{17}	22.7×10^{13}	9	32.5×10^{18}	0.08	24.7×10^{-6}
P25	12.5×10^{17}	34.9×10^{13}	7	7.8×10^{18}	0.17	47.2×10^{-6}

[a] Reaction conditions: HMF (1 mM, 0.02 mmol), photocatalyst (1 g L^{-1}, 20 mg), reaction medium (acetonitrile), HMF solution volume (20 mL), reaction time (1 h), incident light wavelength (515 nm), and light intensity [$\approx$54 W m^{-2} ($6\times\approx$9 W m^{-2})]

Mechanistic studies of oxidation of HMF via LMCT-mediated activation of SGH-TiO_2

In order to identify the active species involved in the photocatalytic oxidation of HMF, different scavengers [methanol, 1,4-benzoquinone (BQ), and silver cations] were separately added in the reaction system under the same conditions. The addition of methanol as hole (h^+) trap does not greatly affect the HMF conversion (56%) and DFF selectivity (88%), meaning that h^+ is not the key active species for the photocatalytic oxidation of HMF (entry 8, Table 2). When BQ was added in the reacting suspension as superoxide radical anion ($O_2^{-\bullet}$) scavenger, the conversion of HMF and formation of DFF are completely inhibited (entry 9, Table 2). This is an indication that $O_2^{-\bullet}$ is the leading active species for the photocatalytic oxidation of HMF to DFF. In contrast, the addition of silver cations as electron acceptors totally stopped the photocatalytic activity (entry 10, Table 2). This demonstrates their potential involvement in the formation of active intermediates of HMF oxidation. The above discussion suggests that Ag^+ as electron acceptor may hinder the formation of $O_2^{-\bullet}$, possibly responsible for the oxidation of HMF. Moreover, to evaluate the effect of oxygen, the photocatalytic oxidation of HMF was carried out in anoxic conditions (Ar 25 mL min^{-1} and degassed acetonitrile) as well as by bubbling air (25 mL min^{-1}) into the system. The anoxic conditions greatly influence the photocatalytic activity and impede the conversion of HMF (entry 11, Table 2). In contrast, bubbling air into the photocatalytic system improved the DFF selectivity up to 96% (entry 12, Table 2), although HMF conversion was slightly reduced (52%), which indicates that increased amount of oxygen prevents side reactions possibly by neutralizing the reactive oxygen species (hydroxyl radical) produced by the potential side product (H_2O_2). Moreover, bubbling air may also assist in the desorption of DFF from the catalyst surface, which further improved the DFF selectivity.

To gain further insight about the photocatalytic oxidation of HMF, a number of exploratory experiments were carried out with some commercial catalysts and by changing the reaction conditions. Interestingly, SGH-TiO_2 showed better performance for the selective oxidation of HMF than commercial P25 (entry 3, Table 2). There are a couple of distinct features exhibited by SGH-TiO_2 that may improve its photocatalytic performance. For example, HMF-ads-SGH-TiO_2 showed pronounced shift in the absorption of light from 400 up to 650 nm compared to HMF-ads-P25 (Figure 4). This may have ascribed to higher specific surface area (177 $m^2 g^{-1}$) of SGH-TiO_2 compared to P25 (53 $m^2 g^{-1}$). The higher specific surface area of SGH-TiO_2 provided a greater (4 times) number of potential active sites (OH groups) for the adsorption of HMF, which in turn enhanced the activity of SGH-TiO_2 for the selective oxidation of HMF.

Based on the characterization and photocatalytic experiments carried out in the presence of different scavengers and additives, a reaction pathway for the photocatalytic selective oxidation of HMF to DFF under visible light is proposed (Figure 6). The adsorption of HMF on the surface of SGH-TiO_2 underpins all the photocatalytic oxidation steps. Visible light irradiation activates the LMCT-complex formed by the adsorption of HMF, which inject electrons into the CB of SGH-TiO_2 and transformed HMF to the corresponding radical cation (Step 2, Figure 6). Dissolved oxygen gains an electron from the CB of SGH-TiO_2 and is converted to a superoxide radical anion ($O_2^{-\bullet}$). The radical cation then reacts with the superoxide radical anion and generates hydroperoxyl radical and alkenyl radical (Step 3, Figure 6). In the final step, the hydroperoxyl radical abstracts a hydrogen atom from the alkenyl radical and forms the target product (DFF) and side product (H_2O_2; Step 4, Figure 6). The H_2O_2 produced may adsorb on the SGH-TiO_2 and possibly react with electrons to form a hydroxyl radical, which may also influence the reaction mechanism and DFF selectivity. The radical cation formed in the second step may or may not release into the reaction medium; our experiments cannot distinguish whether the radical cation is released or remains on the surface. If the radical cation remains on the surface, it may react with another HMF molecule and form an alkenyl radical by deprotonation. Subsequently, the superoxide radical anion may attack the alkenyl radical and produce DFF and a hydroperoxide anion. The hydroperoxide anion may react with the proton and form hydrogen peroxide. However, the likelihood of a free radical cation attacked by the superoxide radical anion at the initial step is greater compared to the alkenyl radical attacked at later stages.

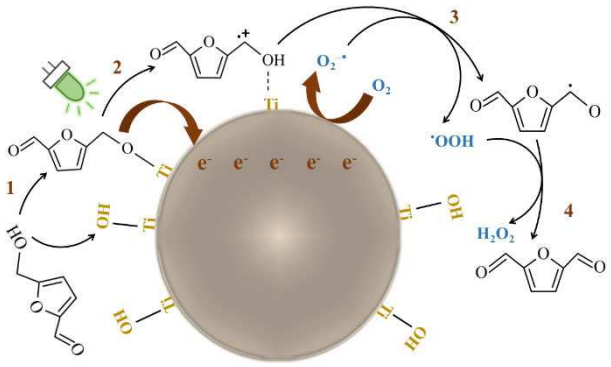

Figure 6. Reaction pathway for the photocatalytic oxidation of HMF over SGH-TiO_2.

Conclusions

The formation of a visible light-active ligand-to-metal charge transfer (LMCT) complex between HMF and titania is shown to enable the photocatalytic selective oxidation of the biomass-derived platform chemical 5-hydroxymethylfurfural (HMF) to the industrially relevant chemical 2,5-diformylfuran (DFF) in the liquid phase. The key step for formation of the LMCT-complex is the dissociative interaction of hydroxyl groups of HMF and the titania surface. However, LMCT occurring in the singlet or triplet state is still elusive as the first triplet state was found approximately 500 nm above the ground singlet state with predicted significantly enhanced accessibility as compared to free HMF. Upon irradiation the LMCT-complex transfers elec-

trons into the conduction band of titania, which react with molecular oxygen in the reaction medium and generate superoxide radical anions responsible for the oxidation of HMF. Generally, the visible light activity of the complex depends on the available surface area of the catalyst, even when the specific surface area of the titania is different. Moreover, the photocatalysts are recyclable and remain highly active over multiple re-uses. The present findings, therefore, show that heterogeneous photocatalysis utilizing widely available titania may have high potential for the valorization of biomass-derived platform chemicals by selective oxidation. This may hold particularly true if the photocatalytic conversion can be accomplished in the presence of visible light with the reactants acting as a sensitizer for titania through formation of a surface complex.

Experimental Section

Chemicals: Titanium(IV) isopropoxide (97+%, Sigma Aldrich), 2-propanol (99.7%, Alfa Aesar), nitric acid (65%, Alfa Aesar), 5-hydroxymethylfurfural (98%, Acros Organics), 2,5-diformylfuran (98%, abcr), titanium(IV) oxide P25 (99.5%, Evonik), acetonitrile (99.9%, POCH), methanol (99.9%, POCH), 1,4-benzoquinone (98%, Sigma Aldrich), silver nitrate (99.8%, STANLAB), anatase (98%, Acros Organics), brookite (99.9%, Sigma Aldrich), sodium fluoride (99%, Chempur), sodium acetate (99.0%, Chempur), potassium trioxalatoferrate(III) trihydrate (98%, abcr), 1,10-phenanthroline (99.5%, Chempur). Water used was purified to 18 MΩ cm resistivity by Milli-Q water purification system.

Synthesis of titania nanoparticles: Titania nanoparticles were synthesized through sol-gel-assisted method adapted from the literature.[62] A TiO_2 sol was prepared by acid-catalyzed hydrolysis of titanium(IV) isopropoxide. In a typical synthesis, specified volume of titanium(IV) isopropoxide (30.5 mL) was dissolved in 2-propanol (25 mL) and stirred for 2 h at room temperature. Subsequently, 1 M HNO_3 (1 mL) was added to the solution under continuous stirring for 5 min until gelation took place. Then, 25 mL of water was slowly added to the gel and stirred for another 3 h. Afterwards, the prepared titania nanoparticles were filtered, washed several times with water, and then dried in an oven at 80 °C for 12 h. The dried sample was ground to powder and transferred to a Teflon-lined autoclave filled (≈80%) with water (50 mL) for hydrothermal treatment at 150 °C for 8 h. Finally, the obtained titania nanoparticles named SGH-TiO_2 were dried at 110 °C in an oven for 12 h.

Synthesis of HMF-adsorbed titania nanoparticles (HMF-Ads-SGH-TiO_2): For the preparation of HMF-Ads-SGH-TiO_2, 20 mg of SGH-TiO_2 was suspended in 1 mM HMF solution (20 mL) in acetonitrile in the glass photoreactor. The suspension was stirred for 1 h in dark at 400 rpm. Afterwards, the catalyst was collected, dried at 80 °C for 3 h, and used for further characterization.

Thermal and chemical modification of titania nanoparticles (SGH-TiO_2): The prepared SGH-TiO_2 nanoparticles were modified further via a thermal and chemical treatment (surface-fluorination) to remove surface-bound OH groups. Thermal treatment involves the calcination of SGH-TiO_2 at 600 °C for 3 h under air with the heating rate of 5 °C min^{-1}.[34] Thermally treated SGH-TiO_2 was named as SGH-TiO_2-cal-600. Surface-fluorinated titania (F-SGH-TiO_2) was prepared according to the method reported in the literature[57] with some modifications. In brief, 0.05 M aqueous solution of NaF was prepared and the pH of the NaF solution was adjusted to 3.5 using HCl. Afterwards, the SGH-TiO_2 (0.06 g) was suspended in 6 mL of NaF solution and stirred for 5 h to fluorinate the SGH-TiO_2 surface. Afterwards, the F-SGH-TiO_2 was collected and dried at 110 °C for 12 h.

Characterization of titania nanoparticles (SGH-TiO_2): Powder XRD measurements were performed employing Bragg-Brentano configuration. This type of arrangement was provided using Empyrean diffraction platform from Malvern PANalytical Co., powered at 40 kV×40 mA and equipped with a vertical goniometer, with theta–theta geometry using Ni filtered CuK_α radiation. Data were collected in range of $2\theta = 9–100°$, with step size of 0.008° and counting time up to 60 s per step. The percentage phase composition of P25 and SGH-TiO_2 was determined through the Rietveld refinements of the XRD patterns. The average crystallite size was determined according to the Scherrer equation [Eq. (1)], where D is the average crystallite size of the catalyst [nm], λ is the wavelength of the CuK_α X-ray radiation ($\lambda = 0.154056$ nm), k is a coefficient usually taken as 0.94, β is the full width at half maximum (FWHM) intensity of the peak observed at 2θ (radian), and θ is the diffraction angle.

$$D = k\lambda/\beta\cos\theta \quad (1)$$

The specific surface area and pore width distribution of the SGH-TiO_2 and P25 was determined through N_2 physisorption isotherms by applying the BET and BJH method, respectively. The measurements were carried out at Micrometrics ASAP 2000 automated system. The FTIR spectrum of SGH-TiO_2 was recorded on Bruker ATR spectrometer in the range of 4000–400 cm^{-1} in transmittance mode with 16 scans and a resolution of 4 cm^{-1}. UV/Vis absorption spectroscopy was performed using a UV/VIS/NIR spectrophotometer Jasco V-570 equipped with an integrating sphere. The baseline was recorded using Spectralon™ [poly(tetrafluoroethylene)] as a reference material. Bandgap values were calculated using Tauc plot applying the Kubelka-Munk function (Figure S12, Supporting Information). The non-polarized Raman spectra were recorded in the back-scattering geometry using in Via Renishaw micro-Raman system equipped with an integrated Leica microscope. As a source of excitation light, the infrared solid-state laser, operating at 785 nm was used. The power of the excitation light was fixed at no more than 20 mW. The laser beam was focused on the sample through the 20×/0.4NA objective. The spatial resolution of the Raman spectra was about 2 μm. The samples were scanned in three spectral range: 100–1000 cm^{-1} (I), 1000–2000 cm^{-1} (II), and 2750–3450 cm^{-1} (III) with the spectral resolution equal to 1 cm^{-1}. The Rayleigh radiation was block by a holographic notch filter. The backscattered Raman light was dispersed by an 1800 mm^{-1} (λ = 785 nm) holographic grating on the Peltier cooled CCD. All measurements were performed at a room temperature. Artefacts from cosmic ray were removed and analyses of the spectra were performed in OPUS (Bruker) software. The leaching of titanium ion after photocatalytic reaction was determined using the energy dispersive X-ray fluorescence analysis (EDXRF) was carried out using MiniPal 4 equipment from PANalytical Co, with a Rh-tube and silicon drift detector (resolution 145 eV) to gain information on the elemental composition of samples. The spectrum was collected in atmosphere, without using a filter, at a tube voltage of 30 kV in order to evaluate the presence of Ti. The time of acquisition was set to 600 s and the tube current up to 50 μA. XPS experiments were performed in a PHI 5000 VersaProbe™ spectrometer (ULVAC-PHI, Chigasaki Japan). The XPS spectra were recorded using monochromatic AlK_α radiation ($h\nu = 1486.6$ eV) from an X-ray source operating at 100 μm spot size, 25 W, and 15 kV. Both survey and high-resolution XPS spectra were collected with the analyzer pass energy of 117.4 and 23.5 eV and the energy step size of 0.4 and 0.1 eV, respectively. Casa XPS software (v.2.3.19, Casa Software Ltd, Wilmslow, United Kingdom) was used to evaluate the XPS data.

Shirley background subtraction and peak fitting with Gaussian-Lorentzian-shaped profiles was performed. Binding energy scale was referenced to the C 1 s peak with a binding energy of 284.8 eV. For quantification, the PHI Multipak sensitivity factors and determined transmission function of the spectrometer were used. The fluorine content of F-SGH-TiO_2 sample was calculated using elemental analyzer (UNICUBE).

OH group density measurement: The OH group density of SGH-TiO_2 and P25 was determined via a TGA weight loss (Figure S4, Supporting Information), performed using a thermobalance (Mettler Toledo TGA/DSC 3+). The method employed for TGA analysis[63,64] involved two steps. In step 1, the sample was heated under air (40 mL min^{-1}) from 25 to 120 °C at 5 °C min^{-1} and held at this temperature for 3 h to remove physically bound water from the surface. In step 2, the temperature was increased to 750 °C at 10 °C min^{-1} and held for 1 h. The mass loss during step 2 was used to calculate the number of hydroxyl groups per surface area according to the following formula [Eq. (2)]:[43]

$$\text{OH nm}^{-2} = \alpha \frac{2(m_T - m_C)\frac{N_A}{M_{H_2O}}}{10^{18} \times \text{ SSA}} \quad (2)$$

Where m_T is the mass loss per mg of the sample between 120 and 750 °C, m_C is the mass loss per mg of the sample due to carbon content (on the basis of evolved CO_2), SSA is specific surface area [$m^2 g^{-1}$], M_{H_2O} is the molar mass of H_2O [g mol^{-1}], α is the calibration constant (0.625),[43,64] and N_A is Avogadro's constant [mol^{-1}].

The carbon content in SGH-TiO_2 and P25 was determined through temperature programmed oxidation (TPO) experiments. The samples were heated at 5 °C min^{-1} from 25 to 120 °C in an oxidative environment (air; 25 mL min^{-1}), with the holdup time of 3 h. After that, samples were cooled down to room temperature and then heated from 25 to 750 °C with the ramp of 10 °C min^{-1} (air: 25 mL min^{-1}). The oxidation process was analyzed by quadrupole mass spectrometer (QMS) Dycor Ametek. The amount of carbon calculated from the CO_2 signals (Figure S13, Supporting Information) of the QMS, calibrated using CO_2 (with the pulse of 1.01×10^{-5} mol).

Photocatalytic selective oxidation of HMF: The photocatalytic reaction was carried out in a glass photoreactor (20 mL). In a typical run, 20 mL of 1 mM (0.02 mmol) HMF solution prepared in acetonitrile and 20 mg of SGH-TiO_2 photocatalyst (1 g L^{-1}) was charged into a glass photoreactor. Subsequently, the suspension was stirred (400 rpm) for 60 min in the dark to attain the equilibrium. The photocatalytic reaction was commenced with the irradiation of green LED lamp ($\lambda = 515$ nm). The photo-intensity of the LEDs was measured to be approximately 54 W m^{-2} ($6 \times \approx 9$ W m^{-2}), recorded by Delta OHM HD 2302.0 light meter with LP 471 RAD probe having a spectral range of 400–1050 nm. The distance between the light source and the wall of the reactor is approximately 2 mm. At given irradiation time intervals, 0.15 mL aliquots were collected and then filtered through a nylon filter (pore size 0.2 μm) to remove the catalyst.

After each run the catalyst was recovered by decanting the solvent, washed several times with water, dried at 110 °C for 48 h, and reused for next cycle with a fresh HMF solution. This process was repeated up to five times of application.

The quantitative analysis of reactants and products was performed on a HPLC instrument (Waters 2487) equipped with a C18 Thermo scientific (250 × 4.6 mm) column using an eluent consisting of 55% acetonitrile and 45% Milli-Q water at a flow rate of 1 mL min^{-1}. The column oven temperature was kept at 25 °C. The HMF conversion [Eq. (3)], DFF selectivity [Eq. (4)], and DFF yield [Eq. (5)] were calculated as follows:

$$\text{HMF conversion} = \frac{M^0_{HMF} - M_{HMF}}{M^0_{HMF}} \times 100 \quad (3)$$

$$\text{DFF selectivity} = \frac{M_{DFF}}{M^0_{HMF} - M_{HMF}} \times 100 \quad (4)$$

$$\text{DFF yield} = \frac{M_{DFF}}{M^0_{HMF}} \times 100 \quad (5)$$

Where M^0_{HMF} corresponds to the initial amount of HMF [mmol], whereas M_{HMF} and M_{DFF} refer to the mmol of HMF and mmol of DFF after the photocatalytic reaction, respectively.

Active sites and conversion per surface OH group: The number of OH groups and conversion of HMF with respect to area and active sites of SGH-TiO_2 and P25 were calculated as follows [Eqs. (6)–(10)]:

$$\text{area} - \text{normalized conversion} = \frac{\text{number of molecules of HMF}_{\text{conv.}}}{\text{SSA} \times m_{cat}} \quad (6)$$

$$\text{area} - \text{normalized rate} = \frac{\text{number of molecules of HMF}_{\text{conv.}}}{\text{SSA} \times m_{cat} \times t} \quad (7)$$

$$\text{number of OH groups} = D_{OH} \times \text{ SSA } \times m_{cat} \quad (8)$$

$$\text{conv. per surface OH groups} = \frac{\text{number of molecules of HMF}_{\text{conv.}}}{\text{number of OH groups}} \quad (9)$$

$$\text{conv. per surface OH groups per unit time} = \frac{\text{number of molecules of HMF}_{\text{conv.}}}{\text{number of OH groups} \times t} \quad (10)$$

where area-normalized conversion is conversion of HMF per m^2 of the catalyst [m^{-2}], area-normalized rate is conversion of HMF per m^2 per unit time [$m^{-2} s^{-1}$], SSA is the specific surface area [$m^2 g^{-1}$], m_{cat} is the mass of the catalyst [g], and D_{OH} is the density of OH groups per m^2.

Apparent quantum yield measurement: The AQY (Φ) for the DFF production is defined as a ratio of the amount of DFF produced per unit time to the number of moles of photon absorbed by the system per unit time [Eq. (11)]:

$$\Phi = \frac{\text{number of moles of DFF produced per unit time}}{\text{number of moles of photons absorbed per unit time}} \times 100 \quad (11)$$

To measure the AQY, the photon flux to the photoreactor was determined by potassium ferrioxalate actinometry.[65–68] The actinometry experiments were performed in a dark room using 515 nm LED with an intensity of approximately 54 W m^{-2} ($6 \times \approx 9$ W m^{-2}). Briefly, 20 mL of 0.15 M potassium ferrioxalate solution was fed into a glass photoreactor used for photocatalytic experiments. Then the actinometer solution was irradiated for 30 s while stirring at the speed of 400 rpm. Simultaneously, another sample prepared with

the same procedure was left in the dark as a control. Upon completion of irradiation an aliquot of 0.15 M potassium ferrioxalate was taken in glass vials and 500 μL of the 0.1% buffered phenanthroline solution was added to irradiated and non-irradiated samples. The samples were then allowed to develop in the dark for 0.5 h. Afterwards, the absorption of each of the sample was measured at 510 nm on Thermoscientific Evolution 220 UV/Vis spectrophotometer. The amount of Fe^{2+} produced during the irradiation was determined using the optical difference (ΔA_{510nm}) between the irradiated and control (dark) sample and the extinction coefficient at 510 nm ($\varepsilon = 11100\ M^{-1}cm^{-1}$).

Knowing that the quantum yield for Fe^{2+} production is 1.0 and that the samples absorb >99% of the incident light, the photon flux absorbed by the sample per unit time was calculated using the following formula [Eq. (12)]:[68]

$$\frac{Nh\nu}{t} = \frac{\text{moles of } Fe^{2+}}{\Phi\ t\ F} \tag{12}$$

where t is the irradiation time in seconds and F is the fraction of light absorbed, which is unity in this case (Figure S14, Supporting Information). Whereas, Nhν refers to number of moles of photon absorbed in einstein.

Quantum chemical calculations: A H-saturated cluster model $[Ti_{20}O_{62}H_{44}]^0$ was used to represent the TiO_2 anatase (101) surface. Such quantum model was extracted from the experimental crystal structure according to the procedure depicted in the Figure S8, Supporting Information. Pure cluster (surface model) was partially relaxed by fixing terminal OH groups Cartesian coordinates to remove bias towards relaxation to thermodynamically more stable rutile-like structure.[69] Various HMF adsorption modes were tested with economic GFN2-xTB method of Grimme and co-workers;[70] in these calculations the HMF was fully relaxed while the surface model was only partially relaxed (see above). The most stable isomers were subject to further geometry refinement at the DFT level using PBE functional,[71,72] def2-SVP basis set,[73] and two corrections: D3BJ[74,75] and gCP,[76] to account for missing dispersion interactions and basis set deficiencies, respectively. Here, the same Cartesian fixing procedure as for GFN2-xTB was applied. Subsequently, single-point calculations were performed with the hybrid PBE0 functional.[77] As a reference, we also performed single-point calculations with the state-of-the-art coupled cluster singles, doubles, and perturbative triples method in the domain localized pair natural orbital approximate formulation [DLPNO-CCSD(T)].[52,53] We note that the method allows to obtain "chemically accurate" (error of <1 kcal mol^{-1}) energetics only at moderately higher cost than DFT. In this computations, the complete basis set limit (CBS) was approximated in a three-step procedure. First, DLPNO-CCSD(T) calculations were performed with the def2-SVP basis set [this yields accurate correlation energy with def2-SVP basis $E(\text{corr})_{CC}^{\text{def2-SVP}}$]. In the next step, MP2 calculations were performed with def2-SVP and def2-TZVP basis sets in order to obtain approximate correlation energies at these basis sets that can be used in two-point extrapolation scheme[78] to get MP2 correlation energy at the CBS limit [these values are denoted as $E(\text{corr})_{MP2}^{\text{def2-SVP}}$, $E(\text{corr})_{MP2}^{\text{def2-TZVP}}$, and $E(\text{corr})_{MP2}^{CBS}$, respectively]. Similarly, one obtains Hartree–Fock correlation energy at the CBS limit (E_{HF}^{CBS}). Finally, DLPNO-CCSD(T)/CBS energy is estimated as:[79]

$$E\left(\text{DLPNO}\frac{\text{CSSD(T)}}{\text{CBS}}\right) \approx E_{HF}^{CBS} + E(\text{corr})_{CC}^{\text{def2-SVP}} + [E(\text{corr})_{MP2}^{CBS} - E(\text{corr})_{MP2}^{\text{def2-SVP}}] \tag{13}$$

Numerical partial Hessian[80] was evaluated with PBE functional at PBE-optimized structures to obtain zero-point energy corrections that were added to the final single-point energies. These calculations were also used to approximate IR and Raman spectra in the 1000–2000 cm^{-1} spectral envelope that is free from frozen OH vibrations. Plotted spectra were broadened using Lorentzian function with half-width of 50 cm^{-1}.

If not stated otherwise, the reported energies are DLPNO-CCSD(T)/CBS + ZPE energies. Comparison of energetics obtained at the DFT + ZPE and MP2 + ZPE levels is provided in Table S2, Supporting Information.

Spin-orbit coupling (SOC) matrix elements were computed with complete active space self-consistent field (CASSCF) method.[81] Initial orbitals were based on a converged triplet PBE0 natural orbitals. A minimal active space was selected with two singly occupied molecular orbitals and two electrons. SOC matrix elements were estimated using the quasi-degenerate perturbation theory.[82]

Coulomb and exact exchange integrals were evaluated with RI[83] and COSX[84] approximations, respectively. Def2 family „/J" and „/C" auxiliary basis sets were applied.[85] DLPNO calculations were performed with TightPNO settings as suggested for weak interactions.[86] All calculations were performed with ORCA 4.2.0 suite of programs.[87]

Acknowledgements

This publication is part of a project that has received funding from the European Union's Horizon 2020 research and innovation programme under the Marie Skłodowska-Curie grant agreement No. 711859 and from the financial resources for science in the years 2017–2021 awarded for the implementation of an international co-financed project. Roger Gläser and Michael Goepel gratefully acknowledges support from the Leipzig Graduate School of Natural Sciences: Building with Molecules and Nano-objects as well as from the Research Academy Leipzig. Adam Kubas acknowledges support from the National Science Centre, Poland, grant number 2018/30/E/ST4/00004. Access to high performance computing resources was provided by the Interdisciplinary Centre for Mathematical and Computational Modelling in Warsaw, Poland, under grant GB79-5. Moreover, authors also acknowledge Ms. Agnieszka Wiśniewska (Soft Matter Research group, IPC PAS) and Mr. Kamil Sobczak (Faculty of Chemistry, Biological and Chemical Research Centre, University of Warsaw) for TGA and TEM measurement, respectively.

Conflict of Interest

The authors declare no conflict of interest.

Keywords: 5-hydroxymethylfurfural · biomass valorization · photocatalysis · titania · visible light

[1] X. Liu, X. Duan, W. Wei, S. Wang, B.-J. Ni, *Green Chem.* **2019**, *21*, 4266.
[2] J. C. Colmenares, R. Luque, *Chem. Soc. Rev.* **2014**, *43*, 765.
[3] S.-H. Li, S. Liu, J. C. Colmenares, Y.-J. Xu, *Green Chem.* **2016**, *18*, 594.

[4] T. Wang, M. W. Nolte, B. H. Shanks, *Green Chem.* **2014**, *16*, 548.
[5] Z. Zhang, G. W. Huber, *Chem. Soc. Rev.* **2018**, *47*, 1351.
[6] T. Su, D. Zhao, Y. Wang, H. Lü, R. S. Varma, C. Len, *ChemSusChem* **2020**, DOI: https://doi.org/10.1002/cssc.202002232.
[7] P. Pal, S. Saravanamurugan, *ChemSusChem* **2019**, *12*, 145.
[8] M. Chatterjee, T. Ishizaka, A. Chatterjee, H. Kawanami, *Green Chem.* **2017**, *19*, 1315.
[9] W. Jia, J. Du, H. Liu, Y. Feng, Y. Sun, X. Tang, X. Zeng, L. Lin, *J. Chem. Technol. Biotechnol.* **2019**, *94*, 3832.
[10] D. A. Giannakoudakis, V. Nair, A. Khan, E. A. Deliyanni, J. C. Colmenares, K. S. Triantafyllidis, *Appl. Catal. B* **2019**, *256*, 117803.
[11] C. Ayed, W. Huang, G. Kizilsavas, K. Landfester, K. A. I. Zhang, *ChemPhotoChem* **2020**, https://doi.org/10.1002/cptc.202000070.
[12] S. Xu, P. Zhou, Z. Zhang, C. Yang, B. Zhang, K. Deng, S. Bottle, H. Zhu, *J. Am. Chem. Soc.* **2017**, *139*, 14775.
[13] Z. Zhang, K. Deng, *ACS Catal.* **2015**, *5*, 6529.
[14] V. R. Battula, A. Jaryal, K. Kailasam, *J. Mater. Chem. A* **2019**, *7*, 5643.
[15] H. Zhang, Q. Wu, C. Guo, Y. Wu, T. Wu, *ACS Sustainable Chem. Eng.* **2017**, *5*, 3517.
[16] I. Krivtsov, E. I. García-López, G. Marcì, L. Palmisano, Z. Amghouz, J. R. García, S. Ordóñez, E. Díaz, *Appl. Catal. B* **2017**, *204*, 430.
[17] Q. Wu, Y. He, H. Zhang, Z. Feng, Y. Wu, T. Wu, *Mol. Cancer* **2017**, *436*, 10.
[18] M. Ge, Q. Li, C. Cao, J. Huang, S. Li, S. Zhang, Z. Chen, K. Zhang, S. S. Al-Deyab, Y. Lai, *Adv. Sci.* **2017**, *4*, 1600152.
[19] G. Zhang, G. Kim, W. Choi, *Energy Environ. Sci.* **2014**, *7*, 954.
[20] S. P. Pitre, T. P. Yoon, J. C. Scaiano, *Chem. Commun.* **2017**, *53*, 4335.
[21] S. Yurdakal, B. S. Tek, O. Alagöz, V. Augugliaro, V. Loddo, G. Palmisano, L. Palmisano, *ACS Sustainable Chem. Eng.* **2013**, *1*, 456.
[22] X. Zhang, L. Lei, *Mater. Lett.* **2008**, *62*, 895.
[23] S. Klosek, D. Raftery, *J. Phys. Chem. B* **2001**, *105*, 2815.
[24] H. She, H. Zhou, L. Li, L. Wang, J. Huang, Q. Wang, *ACS Sustainable Chem. Eng.* **2018**, *6*, 11939.
[25] J. B. Varley, A. Janotti, C. G. Van de Walle, *Adv. Mater.* **2011**, *23*, 2343.
[26] Y. Wang, Y. Wang, Y. Meng, H. Ding, Y. Shan, X. Zhao, X. Tang, *J. Phys. Chem. C* 2008, 112, 6620.
[27] L. Kuang, W. Zhang, *RSC Adv.* 2016, 6, 2479.
[28] J. Lim, A. D. Bokare, W. Choi, *RSC Adv.* 2017, *7*, 32488.
[29] H. Kim, J. Kim, W. Kim, W. Choi, *J. Phys. Chem. C* **2011**, *115*, 9797.
[30] J.-L. Shi, H. Hao, X. Li, X. Lang, *Catal. Sci. Technol.* **2018**, *8*, 3910.
[31] A. G. Agrios, K. A. Gray, E. Weitz, *Langmuir* **2004**, *20*, 5911.
[32] A. G. Agrios, K. A. Gray, E. Weitz, *Langmuir* **2003**, *19*, 1402.
[33] S. Higashimoto, N. Kitao, N. Yoshida, T. Sakura, M. Azuma, H. Ohue, Y. Sakata, *J. Catal.* **2009**, *266*, 279.
[34] S. Higashimoto, K. Okada, M. Azuma, H. Ohue, T. Terai, Y. Sakata, *RSC Adv.* **2012**, *2*, 669.
[35] X. Jiang, M. Manawan, T. Feng, R. Qian, T. Zhao, G. Zhou, F. Kong, Q. Wang, S. Dai, J. H. Pan, *Catal. Today* **2018**, *300*, 12.
[36] M. Zhao, L. Li, H. Lin, L. Yang, G. Li, *Chem. Commun.* **2013**, *49*, 7046.
[37] M. Thommes, *Chem. Ing. Tech.* **2010**, *82*, 1059.
[38] R. Boppella, P. Basak, S. V. Manorama, *ACS Appl. Mater. Interfaces* **2012**, *4*, 1239.
[39] S. Dai, Y. Wu, T. Sakai, Z. Du, H. Sakai, M. Abe, *Nanoscale Res. Lett.* **2010**, *5*, 1829.
[40] T. Huyen, T. Chi, N. Dung, H. Kosslick, N. Liem, *Nanomaterials* **2018**, *8*, 276.
[41] C.-Y. Wu, K.-J. Tu, J.-P. Deng, Y.-S. Lo, C.-H. Wu, *Materials* **2017**, *10*, 566.
[42] D. Zhao, C. Chen, Y. Wang, H. Ji, W. Ma, L. Zang, J. Zhao, *J. Phys. Chem. C* **2008**, *112*, 5993.
[43] A. K. Kharade, S. Chang, *J. Phys. Chem. C* **2020**, *124*, 10981.
[44] J. Guo, X. Cai, Y. Li, R. Zhai, S. Zhou, P. Na, *Chem. Eng. J.* 2013, 221, 342.
[45] G. Tsilomelekis, T. R. Josephson, V. Nikolakis, S. Caratzoulas, *ChemSusChem* **2014**, *7*, 117.
[46] T. Kim, R. S. Assary, L. A. Curtiss, C. L. Marshall, P. C. Stair, *J. Raman Spectrosc.* **2011**, *42*, 2069.
[47] T. Kim, R. S. Assary, C. L. Marshall, D. J. Gosztola, L. A. Curtiss, P. C. Stair, *Chem. Phys. Lett.* **2012**, *531*, 210.
[48] S. Sahoo, A. K. Arora, V. Sridharan, *J. Phys. Chem. C* **2009**, *113*, 16927.
[49] G. A. Tompsett, G. A. Bowmaker, R. P. Cooney, J. B. Metson, K. A. Rodgers, J. M. Seakins, *J. Raman Spectrosc.* **1995**, *26*, 57.
[50] B. Bharti, S. Kumar, H.-N. Lee, R. Kumar, *Sci. Rep.* **2016**, *6*, 32355.
[51] T. Petersen, T. Klüner, *Z. Phys. Chem.* **2020**, *234*, 813.
[52] C. Riplinger, F. Neese, *J. Chem. Phys.* **2013**, *138*, 034106.
[53] C. Riplinger, B. Sandhoefer, A. Hansen, F. Neese, *J. Chem. Phys.* **2013**, *139*, 134101.
[54] A. Kubas, D. Berger, H. Oberhofer, D. Maganas, K. Reuter, F. Neese, *J. Phys. Chem. Lett.* **2016**, *7*, 4207.
[55] H. Xiao, J. Tahir-Kheli, W. A. Goddard, *J. Phys. Chem. Lett.* **2011**, *2*, 212.
[56] J. Kallioinen, G. Benkö, V. Sundström, J. E. I. Korppi-Tommola, A. P. Yartsev, *J. Phys. Chem. B* **2002**, *106*, 4396.
[57] J. S. Park, W. Choi, *Langmuir* **2004**, *20*, 11523.
[58] B. Ohtani, *Chem. Lett.* **2008**, *37*, 216.
[59] B. Ohtani, *Front. Chem.* **2017**, *5*.
[60] M. Melchionna, P. Fornasiero, *ACS Catal.* **2020**, *10*, 5493.
[61] S. E. Braslavsky, A. M. Braun, A. E. Cassano, A. V. Emeline, M. I. Litter, L. Palmisano, V. N. Parmon, N. Serpone, *Pure Appl. Chem.* **2011**, *83*, 931.
[62] A. Tawari, W.-D. Einicke, R. Gläser, *Catalysts* **2016**, *6*, 31.
[63] A. Spyrogianni, I. K. Herrmann, K. Keevend, S. E. Pratsinis, K. Wegner, *J. Colloid Interface Sci.* **2017**, *507*, 95.
[64] R. Mueller, H. K. Kammler, K. Wegner, S. E. Pratsinis, *Langmuir* **2003**, *19*, 160.
[65] F. F. Marafatto, M. L. Strader, J. Gonzalez-Holguera, A. Schwartzberg, B. Gilbert, J. Peña, *Proc. Natl. Acad. Sci. USA* **2015**, *112*, 4600.
[66] C. G. Hatchard, C. A. Parker, *Proc. R. Soc. London. Ser. A* **1956**, *235*, 518.
[67] Y. Quan, S. O. Pehkonen, M. B. Ray, *Ind. Eng. Chem. Res.* 2004, 43, 948.
[68] S. P. Pitre, C. D. McTiernan, W. Vine, R. DiPucchio, M. Grenier, J. C. Scaiano, *Sci. Rep.* **2015**, *5*, 16397.
[69] Z.-H. Cui, F. Wu, H. Jiang, *Phys. Chem. Chem. Phys.* **2016**, *18*, 29914.
[70] C. Bannwarth, S. Ehlert, S. Grimme, *J. Chem. Theory Comput.* **2019**, *15*, 1652.
[71] J. P. Perdew, K. Burke, M. Ernzerhof, *Phys. Rev. Lett.* 1996, 77, 3865.
[72] J. P. Perdew, K. Burke, M. Ernzerhof, *Phys. Rev. Lett.* 1997, 78, 1396.
[73] A. Schäfer, H. Horn, R. Ahlrichs, *J. Chem. Phys.* **1992**, *97*, 2571.
[74] S. Grimme, J. Antony, S. Ehrlich, H. Krieg, *J. Chem. Phys.* **2010**, *132*, 154104.
[75] S. Grimme, S. Ehrlich, L. Goerigk, *J. Comput. Chem.* **2011**, *32*, 1456.
[76] H. Kruse, S. Grimme, *J. Chem. Phys.* **2012**, *136*, 154101.
[77] C. Adamo, V. Barone, *J. Chem. Phys.* **1999**, *110*, 6158.
[78] Y. Minenkov, E. Chermak, L. Cavallo, *J. Chem. Theory Comput.* **2015**, *11*, 4664.
[79] P. Jurečka, J. Šponer, J. Černý, P. Hobza, *Phys. Chem. Chem. Phys.* **2006**, *8*, 1985.
[80] H. Li, J. H. Jensen, *Theor. Chem. Acc. Theory, Comput. Model. (Theoretica Chim. Acta)* **2002**, *107*, 211.
[81] B. O. Roos, P. R. Taylor, P. E. M. Sigbahn, *Chem. Phys.* **1980**, *48*, 157.
[82] D. Ganyushin, F. Neese, *J. Chem. Phys.* **2006**, *125*, 024103.
[83] K. Eichkorn, O. Treutler, H. Öhm, M. Häser, R. Ahlrichs, *Chem. Phys. Lett.* **1995**, *242*, 652.
[84] R. Izsák, F. Neese, *J. Chem. Phys.* **2011**, *135*, 144105.
[85] F. Weigend, M. Häser, H. Patzelt, R. Ahlrichs, *Chem. Phys. Lett.* **1998**, *294*, 143.
[86] D. G. Liakos, M. Sparta, M. K. Kesharwani, J. M. L. Martin, F. Neese, *J. Chem. Theory Comput.* **2015**, *11*, 1525.
[87] F. Neese, F. Wennmohs, U. Becker, C. Riplinger, *J. Chem. Phys.* **2020**, *152*, 224108.

Manuscript received: November 19, 2020
Revised manuscript received: December 30, 2020
Accepted manuscript online: January 16, 2021
Version of record online: January 21, 2021